Dipolar interactions in arrays of nickel nanowires studied by ferromagnetic resonance

A. Encinas-Oropesa, M. Demand, and L. Piraux
Unité de Physico-Chimie et de Physique des Matériaux, Place Croix du Sud 1, B-1348 Louvain-la-Neuve, Belgium

I. Huynen
Laboratoire d'Hyperfréquences, Université Catholique de Louvain, B-1348 Louvain-la-Neuve, Belgium

U. Ebels
Institut de Physique et Chimie des Matériaux de Strasbourg, F-67037 Strasbourg, France
(Received 28 July 2000; revised manuscript received 30 November 2000; published 15 February 2001)

Using a planar microstrip transmission line, the dipolar interactions in electrodeposited Ni nanowires arrays are characterized as a function of the membrane porosity (4% to 38%) and the wire diameter (56 to 250 nm). The dipolar interactions between the wires can be modeled in a mean-field approach as an effective uniaxial anisotropy field oriented perpendicular to the wire axis and proportional to the membrane porosity. The dipolar interaction field opposes the self-demagnetization field of an isolated single wire which keeps the magnetization parallel to the wire axis. An increase in the porosity therefore induces a switching of the effective anisotropy easy axis from parallel to perpendicular to the wire axis above a critical porosity of 35-38% independent of the wire diameter.

DOI: 10.1103/PhysRevB.63.104415 PACS number(s): 76.50.+g, 75.30.Gw

I. INTRODUCTION

In recent years the static and dynamic properties of submicron scale magnetic elements have attracted much attention motivated by potential applications in the area of ultrahigh density magnetic recording and by promising magnetotransport properties. An attractive and direct method to prepare large-area 2D arrays of parallel magnetic nanowires consists in electrodepositing into nanometer-wide cylindrical pores of a porous material, such as track-etched polymer membranes and anodic alumina filters. Both templates enable to fabricate magnetic nanowires of uniform diameter and extremely large aspect ratios controlled to a high degree.[1–3]

Besides the static and magneto-transport properties of magnetic nanowire arrays which have been investigated intensively in recent years,[1,4–11] the dynamic properties of magnetic nanostructures are also of considerable interest in both fundamental as well as applied research. For example recent experiments on lithographically defined arrays of magnetic wires and dots using Brillouin light scattering have shown the effect of the lateral confinement on the dynamic mode spectrum as well as the effect of dipolar interactions.[12–14] Similarly, a study of the microwave permeability of composite materials containing submicronic ferromagnetic particles in a dielectric matrix revealed the excitation of spin wave modes.[15]

In this paper, the dipolar interaction fields are characterized for high porosity electrodeposited nanowire arrays using high frequency ferromagnetic resonance (FMR) techniques. In a recent work, we have shown the possibility to excite the uniform mode resonance in arrays of magnetic nanowires at microwave frequencies using a microstrip transmission line.[16] The experimental method consists in measuring the transmission of an incident microwave signal propagating along a microstrip transmission line deposited on one face of a magnetically-filled porous membrane, see Fig. 1(a). The small pore diameter (compared to the skin depth), the insulating nature of the polycarbonate membrane, as well as its geometry make these systems particularly well adapted for a simple fabrication of the microstrip transmission line and the investigation of the ferromagnetic resonance properties at GHz frequencies. Using track-etched polymer membranes, the interwire spacing can be controlled over a range of 0.1 to 10 μm corresponding to areal densities varying between 10^6 to 10^{10} cm^{-2}. This allows one to explore the properties and dipolar interactions between the wires from the limit of isolated towards the limit of almost touching wires. Here, the dipolar interaction between wires grown in membranes of

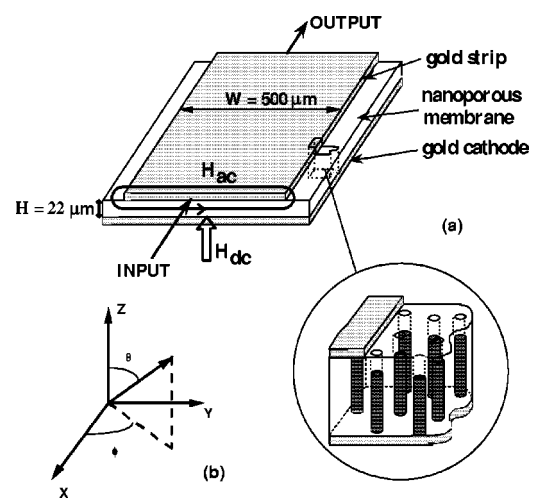

FIG. 1. (a) Schematic description of the strip line transmission line consisting of a metallic ground plane (and cathode), an insulating nanoporous substrate filled with magnetic nanowires and the 500 μm wide metallic strip line and, (b) coordinate system used throughout this article in which the wire axis is parallel to the Z axis.

 ©2001 The American Physical Society

TABLE I. Wire diameter and membrane porosity of the samples used throughout this study.

Sample	Diameter (nm)	Porosity (%)
1	56	4-5
2	95	25-30
3	105	10-12
4	115	12-15
5	180	4-5
6	250	35-38

porosity ranging from 4–5% and up to 35–38% were quantified by studying the angular dependence of the frequency-field dispersion of the uniform mode. It is found that the dipolar interaction field can be described in a mean-field approach by a uniaxial anisotropy field which is proportional to the porosity and which favors an alignment of the magnetization perpendicular to the wires. As a consequence, above a critical value of the porosity a switching of the effective easy axis is induced from parallel to perpendicular to the wire axis.

II. EXPERIMENTAL TECHNIQUE

The arrays of nickel nanowires are synthesized by electrodeposition into track-etched polymer membranes produced at the lab scale.[3] Here, 22 μm thick polycarbonate membranes were used with diameters ranging from 56 nm to 250 nm.

Prior to deposition, a metallic layer of 20 nm Cr and 0.3-1 μm Au serving as the cathode is deposited by evaporation on one face of the template. Electrodeposition of the magnetic nanowires was made at room temperature from a single Ni sulfamate bath in the chronoamperometry mode with the potential fixed at -1.1 V over a surface of 2.5×0.5 cm^2. Deposition is monitored in real time in terms of the deposited charge which allows a precise control of the quantity of the deposited material. Owing to the improved properties the membrane, the electrodeposited nanowires are almost perfectly cylindrical, parallel (deviation is less than $\pm 5°$) and present a very low surface roughness.[3]

Besides Ni arrays inside polymer templates, additional Ni arrays were prepared using as template commercial alumina filters (anodisc).[17] These 60 μm thick filters have a pore diameter of 250 nm and a porosity of $\sim$35–38% which is well above the values obtained currently in polycarbonate membranes.

Table I presents a summary of all the samples used throughout this study, listing the pore diameter and the nominal porosity P, taken as the product of the pore density and the pore surface.

A schematic representation of the microstrip transmission line using magnetically filled nanoporous membranes as a substrate is shown in Fig. 1(a). Details of the arrangement can be found in Ref. 16. The microwave signal propagation along the microstip transmission line produces a microwave pumping field which is perpendicular to the nanowires and induces a precession of the magnetization around the static equilibrium position. At ferromagnetic resonance power is absorbed from the incident microwave signal and the corresponding minimum in the transmitted power is recorded by a network analyzer which can perform frequency sweeps from 100 MHz up to 40 GHz.[16]

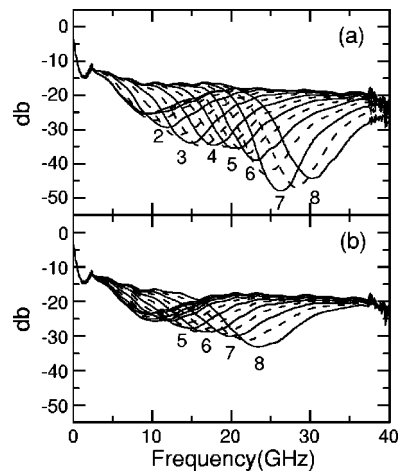

FIG. 2. Microwave absorption spectra as a function of the applied field intensity measured with the field applied (a) parallel and (b) perpendicular to the wires for an array of Ni nanowires of diameter 105 nm and membrane porosity of 12–15%. Measurements were done by decreasing field steps of 500 Oe from 8 kOe down to zero. Continuous lines correspond to integer multiples of the applied field.

The experimental setup has been designed to enable frequency sweeps at applied bias field values H_{AP} varying between ± 8 kOe and for bias field angles θ_H varying between 0 and 180° with respect to the wire axis. For any orientation of the applied bias field, the microwave pumping field and the bias field are kept perpendicular to each other such that the perpendicular FMR pumping configuration is always conserved.

Complementary hysteresis loop measurements have been performed on all samples at room temperature with the field applied parallel and perpendicular to the wires using a SQUID magnetometer.

III. EXPERIMENTAL RESULTS

A. General presentation and features

The microwave transmission line measurements were performed at room temperature for all wire arrays by sweeping the frequency through the resonance peak for fixed applied field direction and strength. This was repeated at constant angle for different field intensities starting from saturation down to zero field. Changing finally the field angle, the full angular dependent frequency-field dispersion was obtained.

Figures 2(a) and 2(b) show typical microwave absorption curves measured on Ni wire arrays as a function of frequency for different values of the static field ($0 \leqslant H_{AP} \leqslant 8$ kOe) applied (a) parallel $\theta = 0°$ and (b) perpendicular $\theta = 90°$ to the wire axis. In this case, the wire diameter is 105 nm and the porosity is 12–15%.

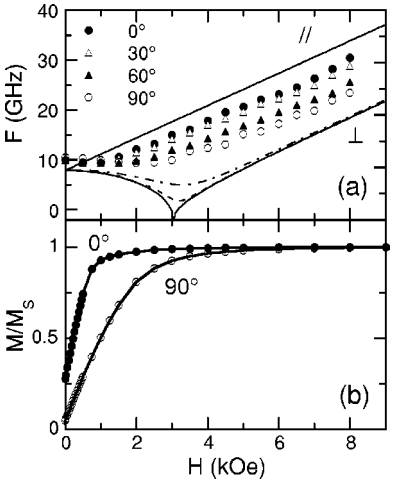

FIG. 3. Measurements performed on an array of Ni nanowires with diameter of 105 nm and membrane porosity of 12–15%. (a) The measured Resonance frequencies as a function of the intensity of the field applied at several directions from the parallel to the wires (0°), the theoretical resonance-field dispersion of isolated wires with the field applied parallel (//) and perpendicular 90°(⊥) to the wires (continuous lines) as well as 89 and 85° (dashed and dashed-dotted lines, respectively) and, (b) corresponding (normalized) hysteresis loops measured at room temperature with the field applied parallel (open circles) and perpendicular (filled circles) to the wires, lines are just a guide to the eyes.

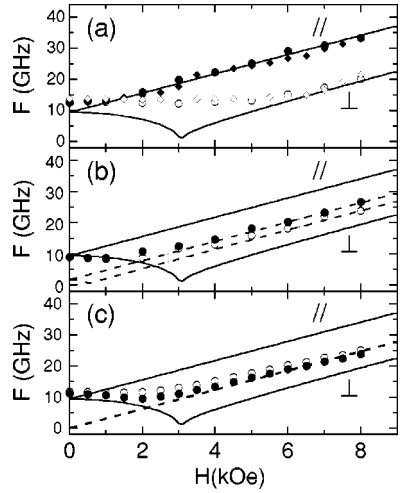

FIG. 4. Resonance frequencies measured in arrays of Ni nanowires with the field applied parallel (filled symbols) perpendicular (open symbols) to the wires. (a) two samples having a porosity of $P=4$–5% and diameters of 56 nm (circles) and 180 nm (diamonds), (b) diameter 95 nm and membrane porosity of 25–27%, (c) diameter is 250 nm and the porosity of the membrane is 35–38%. Continuous lines correspond to the theoretical resonance-field dispersion of isolated wires with the field applied parallel (//) and perpendicular (⊥) to the wires.

It is noted that in order to enhance the signal-to-noise ratio, the original data were numerically smoothened, allowing a clear determination of the absorption minimum and hence of the resonance frequency. As it can be observed, the resonance frequency increases with increasing field but decreases upon rotating the field from the easy to the hard axis. Furthermore, the absorption is observed to be weaker when the field is applied along the hard axis.

From these type of measurements, the angular dependence of the frequency-field dispersion has been extracted as shown in Fig. 3(a) for the same Ni wire array presented in Fig. 2. It can be noticed that the frequency field dispersion presents (for all angles) a high field regime and a low field regime. Upon coming from high fields, the resonance frequency f decreases first linearly with the applied field but remains almost constant below a certain value. The transition field from the high-field regime to the low-field-regime is observed to increase with the angle and can be related to the hysteresis loops as shown in Fig. 3 for $d=105$ nm wires of medium porosity $P=12$–15%. By comparing the frequency-field dispersion for the parallel and perpendicular case, Fig. 3(a), with the corresponding part of the magnetization curves, Fig. 3(b), it is seen that the deviations from the linear regime appear when the sample leaves its saturation state. The same behavior has been observed for all the nanowire arrays considered.

B. Analysis of the absorption properties in the saturation state

First, the linear high field regime is analyzed. This regime corresponds to the saturated state, where the magnetization inside the wires can be considered as single domain and oriented parallel to the applied field direction.

In order to investigate the effects of the dipolar coupling between wires, a set of samples has been prepared with varying membrane porosity. Figure 4 presents the frequency-field dispersion relation measured with the applied field parallel ($\parallel=\theta=0°$) (filled symbols) and perpendicular ($\perp=\theta=90°$) (open symbols) to the wires for (a) two Ni samples having low porosity ($P=4$–5%) and respective wire diameter of 56 nm (circles) and 180 nm (diamonds), (b) Ni wires of diameter 95 nm and membrane porosity of 25–30% and (c) an array of Ni nanowires prepared using an alumina membrane having a pore diameter of 250 nm and a porosity close to 35–38%. It is seen that upon increasing porosity the parallel frequency-field dispersion branch and the perpendicular frequency-field dispersion branch approach each other. In particular, for the case of high porosity, Fig. 4(c), the resonance frequencies are independent of the applied field direction. It is noted furthermore, that the dispersion depends only on the respective porosity and not on the diameter as seen in Fig. 4(a), where the same dispersion curves are obtained for different wire diameters but same membrane porosity.

Consider first the low porosity case, the wires are independent and the absorption peak will correspond to the uniform mode resonance of a single wire. The corresponding resonance condition can be derived from the total free energy density of an infinite cylinder having an effective uniaxial anisotropy field H_{EF} with a uniaxial symmetry parallel to the wire axis:

$$E=MH_{EF}\sin^2\theta-M_sH_{AP}\times[\sin\theta\sin\theta_H\cos(\phi-\phi_H)+\cos\theta\cos\theta_H] \quad (1)$$

with (θ, ϕ) and (θ_H, ϕ_H) the polar and azimuthal angles of the magnetization M and the applied static (or bias) field H_{AP} respectively, see Fig. 1(b).

H_{EF} is the effective anisotropy field which contains, in its most general form, contributions from the shape, magnetocrystalline and/or a magneto-elastic anisotropy. Previous investigations have shown that at room temperature, the dominant contribution is the shape anisotropy[1,18] for low porosity Ni nanowire arrays. Therefore, the effective anisotropy field is given by the shape demagnetization field $H_{EF}=2\pi M_S$.

For the geometry used in the experiment, with the applied field varying in a plane of $\phi_H=0$ from $\theta_H=0°$ to $\theta_H=90°$ to the wire axis, the resonance frequency is obtained from the second derivative of the energy density Eq. (1) by the formalism of Smit and Beljers as:[19]

$$\frac{\omega}{\gamma}=[(H_{EF}\cos 2\theta_o+H_{AP}\cos(\theta_o-\theta_H)) \times(H_{EF}\cos^2\theta_o+H_{AP}\cos(\theta_o-\theta_H))]^{1/2}. \qquad (2)$$

The equilibrium position of the magnetization θ_o is determined from the first derivative of the energy density with respect to θ for each H_{AP}, θ_H. The gyromagnetic ratio γ, taken as positive, is given by $\gamma=g\mu_b/\hbar$ (μ_b is the Bohr magnetic moment). Using $g=2.21$ for Ni[20] yields $\gamma'=\gamma/(2\pi)=3.09$ MHz/Oe.

In Figs. 3(a) and 4, the calculated frequency-field dispersion of isolated wires is shown for all arrays by the continuous lines for the case of $H\|$ and $H\perp$ using the saturation magnetization value Ni ($M_s=485$ emu/cm^3). As it can be seen for the case of low porosity ($P=4\%$), Fig. 4(a), the parallel and perpendicular dispersion is well reproduced by the isolated wire case in the high field linear regime.

Upon increasing the membrane porosity, the measured frequencies deviate strongly from those calculated for isolated wires. The decrease of the resonance frequency in the parallel case $H\|$, Figs. 4(b) and 4(c) and the corresponding increase in the perpendicular case $H\perp$ indicate that the effective uniaxial anisotropy field H_{EF} is reduced as the wires are brought closer to each other. This reduction of the effective anisotropy results from the dipolar coupling between the wires.[21,22] To further confirm this behavior, hysteresis loops have been measured (Fig. 5) on the (a) low porosity ($P=4\%$) and (b) high porosity ($P=33\%$) Ni wire arrays with the magnetic field applied parallel (filled symbols) and perpendicular (open symbols) to the wires.

The magnetization measurements show that for low porosity the hysteresis loops correspond well to those of a highly anisotropic system. The $M(H)$ loop obtained with the field applied parallel to the wires shows a low saturation field and high remanence. Whereas when the field is applied perpendicular to the wires, the hysteresis loop presents a high saturation field and very low remanence. In the case of a high porosity [Fig. 5(b)] we observe the behavior of an isotropic system in which both cycles are identical and in good agreement with the corresponding frequency-field dispersion [Fig. 4(c)].

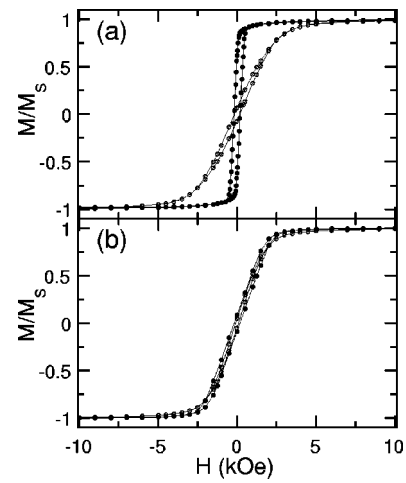

FIG. 5. Normalized Hysteresis loops measured at room temperature with the field applied parallel (filled circles) and perpendicular to the wires (open circles), for Ni nanowires arrays with a diameter of 56 nm (a) and 250 nm (b) and porosity of 4% and 35–38%, respectively. Lines are just guides to the eye.

The effects of the dipolar coupling can be taken into account by including an additional uniaxial anisotropy field H_U which favors an easy axis perpendicular to the wires. The effective anisotropy field is then $H_{EF}=2\pi M_S-H_U$ ($H_U>0$). By introducing this field in Eqs. (1) and (2) it is possible to fit the measured resonance frequencies in the high field regime which yields the dispersion curves indicated by the dashed lines in Figs. 4(b) and 4(c). The corresponding values of the dipolar field H_U are plotted in Fig. 6(a) as a function of the porosity for all the samples considered in this study. It is seen that H_U increases almost linearly with increasing P.

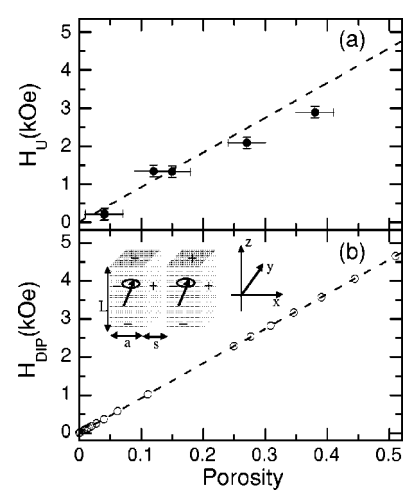

FIG. 6. Dipolar interaction field as a function of the nominal porosity P. In (a) the experimental values (dots) compared with the mean field model $H=6\pi M_S P$ (dashed line). The error bars correspond to $\pm 3\%$ of the nominal porosity and (b) calculated total dipolar interaction for an array of square wires (inset), shown as open circles, compared to the mean field expression (dashed line).

This linear dependence of the dipolar coupling on P can be derived using a phenomenological mean field approach.[23] Upon decreasing the wire separation (increasing P) the wires start to interact via their dipolar stray fields which add to the restoring torque of the individual wires and change the resonance frequency. Besides the self-demagnetizing field $2\pi M_S$, there will be two additional contributions to the restoring torque which are taken proportional to P.[23] First, the charges on the cylindrical wire surfaces produce a dipolar field which opposes the self demagnetization field and can be written in the form of $-2\pi M_S \cdot P$. Second, the charges at the top and bottom extremities give rise to an interaction field of $-4\pi M_S \cdot P$. Combining the two contributions with the wire shape anisotropy, the net magnetostatic field yields

$$\begin{aligned} H_{EF} &= 2\pi M_S - 2\pi M_S P - 4\pi M_S P \\ &= 2\pi M_S(1-3P). \end{aligned} \tag{3}$$

From this equation, the limit of isolated wires is obtained for $P \rightarrow 0$, whereas the continuous film limit is given by $P \rightarrow 1$.

In Fig. 6(a) the experimental fit values (dots) for H_U as a function of P are compared to the dipolar interaction field of Eq. (3) given by $H_U = 6\pi M_S P$ (dashed line). A good agreement is found. The deviations are within the error bars when considering that the real porosity of the system is expected to be slightly lower than the nominal membrane porosity.

The scaling with the porosity of the two contributions to the mean-field dipolar interaction field given in Eq. (3) was verified by calculating numerically the exact static dipolar interaction fields. For this the dipolar stray fields arising from the charges on the cylindrical wire surfaces and from the flat ends of the wire extremities was determined for the two cases that (a) all wires are magnetized perpendicular to the wire axis ($H_{XY\mathrm{tot}}$) and (b) all wires magnetized parallel to the wire axis ($H_{Z\mathrm{tot}}$). For simplicity a square array of infinitely long square wires was chosen as indicated in the inset of Fig. 6(b). The porosity in this case is given by $P = a^2/(a+s)^2$, where a is the side length of a single square wire and s the distance between the wires which was varied from 0 to 50 times a. The stray field components H_{xy} and H_z are obtained from the integral expressions F100 and F110 given in Ref. 24 for homogeneously charged surface sheets of the y-z and x-z side faces and the top and bottom x-y surfaces, respectively. The dipolar fields are then summed over all charged surfaces of the whole array using a maximum number of ± 5000 neighbor cells, which guarantees convergence of the dipolar field sum.

In Fig. 6(b) the exact calculated interaction field $H_{\mathrm{int}} = H_{Z\mathrm{tot}} + H_{XY\mathrm{tot}}$ (open circles) is compared to the expression of Eq. (3) $H_U = 6\pi M_S P$. For the considered porosity range both expressions yield the same field values, confirming that in the mean-field approach, Fig. 6(a), the dipolar interaction field varies linearly with the porosity. It is furthermore noted, that the second form of Eq. (3) shows that for $P = 1/3$ the total effective field is zero, which implies an isotropic behavior. This critical value corresponds very well to the one found from the magnetization and resonance experiments, see Figs. 4(c) and 5(b), at which the microwave absorption as well as the hysteresis loops are independent of the applied field direction.

C. Low field behavior

In the following, the observed deviations from the calculated frequency-field dispersions curves which occur below the saturation field will be briefly addressed.

(i) For fields applied perpendicular to the wire axis, a well defined minimum (zero frequency) is expected when the applied field is equal to the effective anisotropy field, see the full lines Figs. 3(a) and 4. This minimum is not observed in the experiment and can be accounted for, at least partially, to a small inherent misalignment between the applied field and the wire axis. This misalignment is introduced by the experimental setup as well as by a small angular dispersion ($\pm 5°$) of the wire orientation within the porous membrane. In Fig. 3(a), the calculated frequency-field dispersion is shown for $\theta_H = 85°$ and $89°$, dashed-dotted line and dashed line, respectively. Notice that even for a misalignment of one degree, the minimum of the resonance frequency around the saturation field value is substantially suppressed.

(ii) As stated previously, independently of the applied field direction, below the saturation field the resonance frequency shows a field dependence which differs from the one of the uniform mode precession frequency. These differences result from the fact that below the saturation field, the system is no longer single domain. Experimentally, this is supported by the hysteresis loops measured with the field applied parallel to the wires [see Fig. 5(a)], for which the remanent magnetization is lower than the saturation magnetization. Nevertheless, the resonance frequency measured at zero field is found to be almost the same, and very close to 10 GHz, independently of the wire diameter, array porosity or the applied field direction (see Figs. 3 and 4). Furthermore, this frequency is close to the one expected for isolated Ni wires at remanence, which is, $2\gamma' \pi M_S = 9.42$ GHz, suggesting that in the remanent state the dipolar coupling is ''switched off.'' This can be explained by the formation of a multidomain state below the saturation field, which tends to minimize the zero field stray field energy. Consequently, the dynamic dipolar interaction fields between the wires are reduced and the resonance frequency will converge to that of the isolated wires. However, additional studies are necessary to establish the detailed low-field magnetization distribution inside the wires.

IV. CONCLUSION

In conclusion, the ferromagnetic resonance properties of arrays of nickel nanowires have been studied using a microstrip transmission line configuration in the frequency range of 100 MHz up to 40 GHz. By tuning the porosity of the membrane, it is possible to explore the transition from the limit of isolated wires to that of interacting wires. Experimentally, it is shown that the effects of the dipolar coupling can be characterized using this FMR technique. The effective interaction field has been modeled within a mean field ap-

proach with the interaction field expressed as a linear function of the porosity as was verified by exact numerical calculations. The model predicts that, independent of the wire diameter or material, at a porosity of $P=1/3$ the wire array behaves isotropically as confirmed by FMR and hysteresis loops measurements. This mean-field approach remains valid at magnetic field values for which the magnetization is saturated. One remarkable property of these nanowire arrays is that at remanence the resonance frequency is independent of both field history and membrane porosity and given only by the self-demagnetization field ($\omega/\gamma=2\pi M_S$). These type of nanowire arrays might be potentially useful for microwave devices since the absorption frequency range can be tuned simply by varying either the membrane porosity or the material (M_S).

ACKNOWLEDGMENTS

The authors wish to thank R. Legras and E. Ferain for providing the polycarbonate membrane samples used in this work. We express our gratitude to Professor Philip E. Wigen for his valuable remarks and fruitful discussions. I.H. and L.P. are Research Associates of the National Fund for Scientific Research (Belgium). This work was partly supported by the ''Région Wallonne,'' by the Growth Programme GR5D-1999-0135 as well as by the EC-TMR programme no. ERBFMRX-CT97-0124.

[1] For a recent review, see A. Fert and L. Piraux, J. Magn. Magn. Mater. **200**, 338 (1999).

[2] H. Masuda and F. Fukuda, Science **264**, 794 (1994).

[3] E. Ferain and R. Legras, Nucl. Instrum. Methods **B131**, 97 (1997), and references therein.

[4] N. Tsuya, Y. Saito, H. Nakamura, S. Hayano, A. Furugohri, K. Ohta, Y. Wakui, and T. Tokushima, J. Magn. Magn. Mater. **54-57**, 1681 (1986).

[5] K. I. Arai, K. Ishiyama, Y. Ohoka, and H. W. Kang, J. Magn. Soc. Jpn. **13**, 789 (1989).

[6] T. M. Whitney, J. S. Jiang, P. Searson, and C. Chien, Science **261**, 1316 (1993).

[7] L. Piraux, S. Dubois, E. Ferain, R. Legras, K. Ounadjela, J. M. George, J. L. Maurice, and A. Fert, J. Magn. Magn. Mater. **165**, 352 (1997); R. Ferr, K. Ounadjela, J. M. George, L. Piraux, and S. Dubois, Phys. Rev. B **56**, 14066 (1997).

[8] W. Wernsdorfer, B. Doudin, D. Mailly, K. Hasselbach, A. Benoit, J. Meier, J.P. Ansermet, and B. Barbara, Phys. Rev. Lett. **77**, 1873 (1996).

[9] R. O'Barr and S. Schultz, J. Appl. Phys. **81**, 5458 (1997); M. Lederman, R. O'Barr, and S. Schultz, IEEE Trans. Magn. **31**, 3793 (1995); L. Belliard, J. Miltat, A. Thiaville, S. Dubois, J. L. Duvail, and L. Piraux, J. Magn. Magn. Mater. **190**, 1 (1998).

[10] E. Wegrowe, S. E. Gilbert, D. Kelly, B. Doudin, and J. P. Ansermet, IEEE Trans. Magn. **34**, 903 (1998); S. Pignard, G. Goglio, J.L. Duvail, S. Dubois, A. Radulescu, and L. Piraux, J. Appl. Phys. **87**, 824 (2000).

[11] L. Piraux, J. M. George, J. F. Despres, C. Leroy, E. Ferain, R. Legras, K. Ounadjela, and A. Fert, Appl. Phys. Lett. **65**, 2484 (1994).

[12] B. Hillebrands, C. Mathieu, M. Bauer, S.O. Demokritov, B. Bartenlian, C. Chappert, D. Decanini, F. Rousseaux, and F. Carcenac, J. Appl. Phys. **81**, 4993 (1997).

[13] C. Mathieu, J. Jorzick, A. Frank, S.O. Demokritov, A.N. Slavin, B. Hillebrands, B. Bartenlian, C. Chappert, D. Decanini, F. Rousseaux, and E. Cambril, Phys. Rev. Lett. **81**, 3968 (1998).

[14] M. Grimsditch, R. Camley, E.E. Fullerton, S. Jiang, S.D. Bader, and C.H. Sowers, J. Appl. Phys. **85**, 5901 (1999).

[15] G. Viau, F. Fivet-Vincent, F. Fivet, P. Toneguzzo, F. Ravel, and O. Acher, J. Appl. Phys. **81**, 2749 (1997).

[16] G. Goglio, S. Pignard, A. Radulescu, L. Piraux, I. Huynen, D. Vanhoenacker, and A. Vander Vorst, Appl. Phys. Lett. **75**, 1769 (1999).

[17] Whatman S.A., Louvain-la-Neuve, Belgium.

[18] S. Dubois, J. Colin, J. L. Duvail, and L. Piraux, Phys. Rev. B **61**, 14315 (2000).

[19] C. Vittoria, *Microwave Properties of Magnetic Films* (World Scientific, Singapore, 1993).

[20] C. Kittel, *Introduction to Solid State Physics*, 6th ed. (Wiley, New York, 1986), p. 482.

[21] M. Lenderman, R. O'Barr, and S. Schultz, IEEE Trans. Magn. **31**, 3793 (1995).

[22] G. J. Strijkers, J. H. Dalderop, M. A. A. Broeksteeg, H. J. M. Swagten, and W. J. M. de Jonge, J. Appl. Phys. **86**, 5141 (1999).

[23] U. Netzelmann, J. Appl. Phys. **68**, 1800 (1990).

[24] A. Hubert and R. Schäfer, *Magnetic Domains* (Springer-Verlag, New York, 1998), p. 122.